Exploration of Interfacial Porphine Coupling Schemes and Hybrid Systems by Bond-Resolved Scanning Probe Microscopy

Felix Bischoff, Yuanqin He, Alexander Riss*, Knud Seufert, Willi Auwärter*, Johannes V. Barth*

Physics Department E20, Technical University of Munich, James-Franck-Str. 1, 85748 Garching, Germany

E-Mail: a.riss@tum.de, wau@tum.de, jvb@tum.de

Abstract The templated synthesis of porphyrin-based oligomers and heterosystems is of considerable interest for materials with tunable electronic gaps, photovoltaic or sensing device elements. Herein, temperature-induced dehydrogenative coupling between unsubstituted free-base porphine units, and their attachment to graphene nanoribbons on a well-defined Ag(111) support are scrutinized by bond-resolved scanning probe microscopy techniques. Our detailed inspection of covalently fused porphine dimers obtained by *in-vacuo* on-surface synthesis clearly reveals atomistic details of coupling motifs, whereby also putative reaction intermediates are identified. Moreover, the covalent attachment of porphines at preferred locations of atomically precise armchair-type graphene nanoribbons is demonstrated.

The make of molecular nanostructures at interfaces concomitant with the direct identification of bonding schemes and intramolecular features by scanning probe microscopy is a burgeoning research domain.[1–14] In particular, bond-resolved imaging in noncontact atomic force microscopy (nc-AFM)[1–3,6–8] and scanning tunneling microscopy (STM)[7,9–13] can be achieved by tip-functionalization with molecules, most notably with carbon monoxide (CO).[1,15]

Recently, not only an impressive variety of carbon-based constructs has been reported,[16–23] but also their use to obtain heterostructures including nitrogenated entities.[24–26] Free-base porphine (2H-P) is an appealing building block in this domain. It represents the essential porphyrin unit consisting of the tetrapyrrole macrocycle (cf. model Figure 1c). Due to its simplicity and comparably low number of atoms, it is often implemented as starting point for theoretical studies, e.g., addressing metalation and other phenomena.[27] Porphines are ideally suited for experimental studies of fundamental characteristics of surface-anchored porphyrins and to clarify the influence of (meso-)substituents.[28–31] Additionally, 2H-P itself is a very interesting module for two- and three-dimensional nanoarchitectures.[32,33] Conjugated one-dimensional arrays of porphine macrocycles – so called porphine tapes – have been recognized as light-harvesting material exhibiting a steadily decreasing band gap as a function of tape length[34–36] while simultaneously featuring interesting non-linear optical properties.[37,38] To date, porphyrin oligomers have been usually synthesized and characterized in solution-based approaches.[39,40] However, especially for (opto-)electronic applications it is desirable to directly contact the molecular entities with conducting (metal) electrodes for their integration in electrical circuits. Importantly, the molecule-electrode interface can influence molecular properties through charge transfer,[41] conformational adaptations[42,43] and other effects. Accordingly, characterization in a well-defined ultra-high-vacuum UHV environment is desirable for understanding molecular systems with promise as building blocks in molecular electronic or other devices.

The integration of tetrapyrroles in hybrid systems has been demonstrated recently with species connected to graphene nanoribbons[44,45] and their covalent attachment to graphene edges through dehydrogenative coupling.[36] With the latter system, the edge irregularity of graphene islands on Ag(111) interferes and multiple coupling configurations coexist, whereby quantitative investigation of the electronic properties is difficult.[36,46–49] Graphene nanoribbons (GNRs) can have a tunable band gap that is dependent on their width,[50,51] which is crucial for graphene-based electronic applications. Because of such exceptional properties, extensive efforts have been dedicated to the formation of GNRs with atomically precise edge terminations.[16,51] GNRs, such as 7-armchair GNRs (7-AGNRs) with armchair terminations at the long sides and zigzag terminations at the short ends,[16] are ideal candidates to investigate the coupling behavior of porphines to graphene edges, as well as the electronic properties of the coupling junction.

Firstly, we address the imaging and covalent coupling of porphine species. Unlike many porphyrin derivatives,[43] porphines do not self-assemble into regular organic islands, but appear as individual units on

Ag(111) as depicted in Figure 1e, which reflects repulsive molecule-molecule interactions.[41] In STM the macrocycle is resolved square-like with two protrusions and a central depression (cf. Figure 1a,e). The protrusions are associated with the electronic fingerprints of the inner hydrogens,[41] but do not represent a topographic effect as encountered with saddle-shaped 2H-TPP[42] and other poprhine species.[28] In fact, 2H-P adsorbs flat with the macrocycle coplanar to the surface, which manifests as uniform contrast across the entire molecule in constant-height nc-AFM measurements using CO-functionalized tips[1,52,53] (Figure 1b,c). The frequency shift (Δf) maps show the macrocycle bonding scheme, where five-member pyrrole rings are interconnected by kinks corresponding to the methine bridges. Interestingly, the inner hydrogens cannot be clearly identified and 2H-P appears essentially fourfold symmetric in nc-AFM contrasting the electronic structure effects breaking the symmetry in STM (see sect. S2 in the Supporting Information for more details).

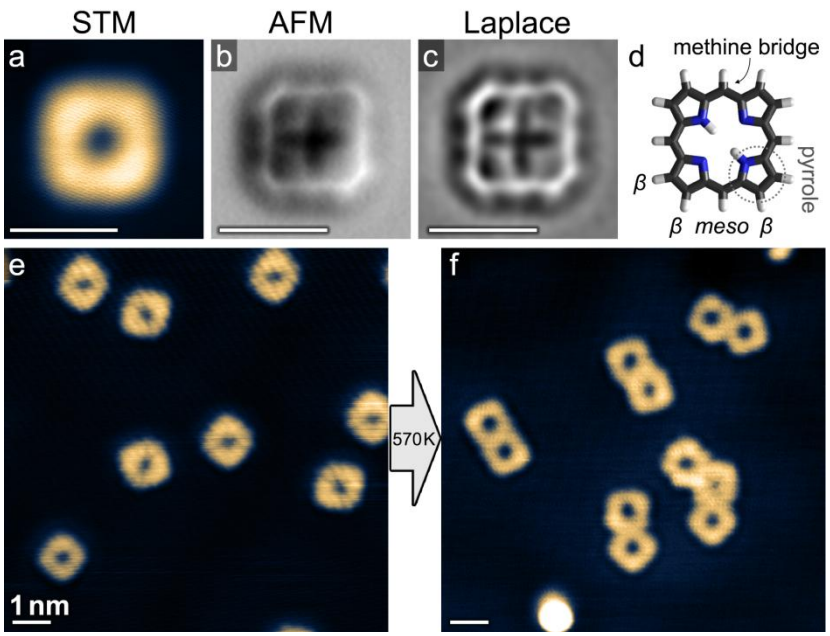

Figure 1. High-resolution imaging of porphine units and coupling products on Ag(111). **(a)** STM image of single 2H-P with square-like appearance. A symmetry break entails protrusions in the upper left and lower right regions of the macrocycle. **(b)** nc-AFM frequency shift (Δf) data and **(c)** Laplace-filtered version. **(d)** Model of 2H-P. Peripheral carbon positions are denoted by "*β*" at pyrrole and "*meso*" at methine moïeties. Pyrrole ring is marked with a dashed circle. **(e)** Overview image showing the distribution of porphine molecules after room temperature deposition. The molecules are observed as separated single units due to repulsive interaction. **(f)** Heating the sample to 570 K induces the formation of covalently coupled oligomers. Scan parameters: (a) V_S = 200mV, I = 70pA; (b) V_S = 0 V, constant height. (e) V_S = 100 mV, I = 80 pA; (f) V_S = 150 mV, I = 10 pA; T = 5 K.

As reported in our previous study,[32] heating a sample with adsorbed pophines to 570 K for 20 min affords a high yield of fused species forming dimers and oligomers as shown in Figures 1f and 2 (detailed statistical analysis of the distribution of reaction products as a function of annealing temperature is given in ref. [32]). The underlying coupling reaction is accompanied by associative hydrogen desorption from the surface at

the employed preparation conditions.[54,55] Thus the synthesis proceeds without surface decoration by spurious byproducts, in contrast to other popular reactions involving halogen leaving groups.[56]

The porphine coupling motifs can be unambigously identified by nc-AFM measurements. Characteristic reaction products are exemplified by the dimeric species shown in Figure 2. Motif 1 (Figure 2a,e,i,m) reflects a dehydrogenation of three neighboring carbon atoms per molecule and the formation of three covalent C–C bonds. The symmetric *β-β* and *meso-meso*, connections (cf. labels in Figure 1d) provide collinear porphine units and thus represent an element for straight oligomers. Motif 2 (*meso-β, β-meso* bonding, Figure 2b,f,j,n) is due to the dehydrogenation of two carbon atoms per molecule forming two covalent C–C bonds. For motifs 1 and 2 the constituent units are oriented along the same direction with respect to the underlying substrate. Binding motif 3 (*β-β, meso-β,* Figure 2c,g,k,o*)* features two covalent C–C bonds between rotated porphine units. Furthermore, motif 4, hypothesized in earlier work,[32] (Figure 2d,h,l,p) presents a single *β-β* bond between two porphines in the same adsorption orientation, whence the units are laterally shifted against each other.

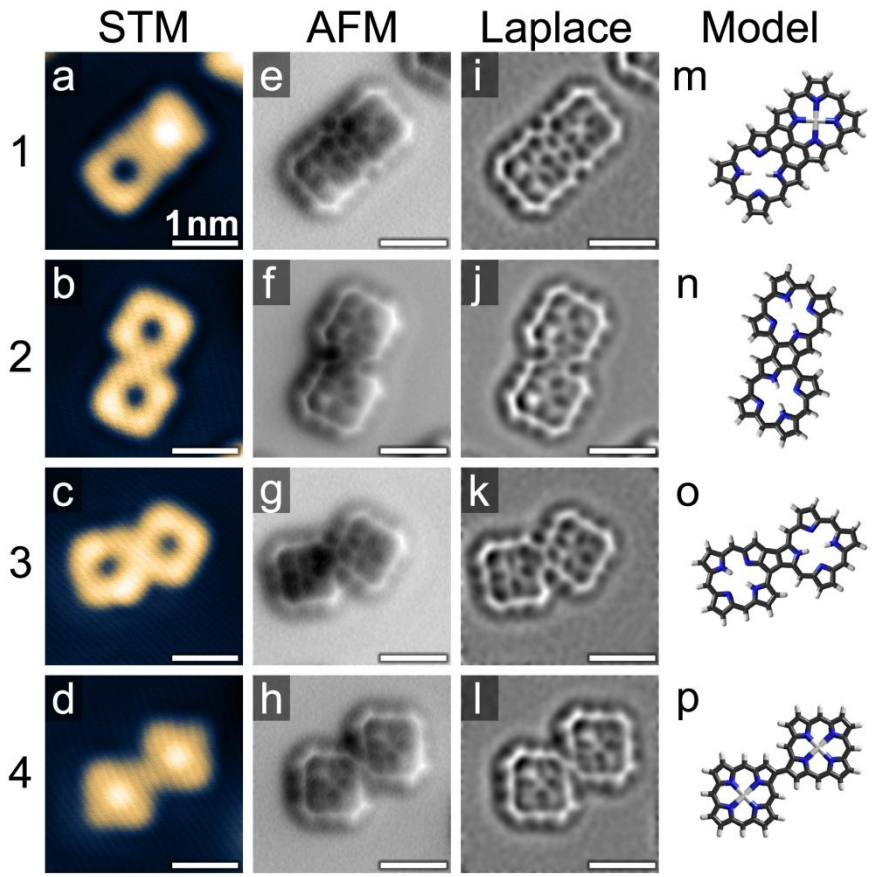

Figure 2. Comparative structure analysis of covalently bonded porphine dimers, which also represent exemplary elements for oligomers. **(a)-(d)** STM images, **(e-h)** AFM Δf images, **(i-l)** Laplace-filtered Δf images, and **(m-p)** the derived chemical structure models of the four observed porphine dimer coupling motifs. Motif 1 is a triple-fused unit with *β-β, meso-meso, β-β* binding. Motif 2 exhibits *meso-β, β-meso* bonding resulting in a lateral offset between the two units. Motif 3 features *β-β, meso-β* bonding with one rotated species. Motif 4 is

a dimer stabilized by a *β*-*β* single bond. Scan parameters: (a) V_S = 200 mV, I = 70 pA; (b)-(d) V_S = 200 mV, I = 50 pA; (e)-(h) V_S = 0 V, constant height; T = 5 K.

Solution-based approaches describe coupling as a multistep process that proceeds via *meso-meso* linked oligomer intermediates[39,57] owing to the higher stability of the *β*-C–H bond compared to the *meso*-C–H bond.[40] Hence the occurrence of motif 4 is ascribed to the surface confinement where C–H bond activation might not be preferred for *meso*-C sites. For surface-assisted porphine oligomerization, the formation of a bond between the *β*-carbons of two porphine units is a likely initial step due to steric reasons. In this configuration one of the constituting units can rotate around the connecting C–C bond and then "flip" toward a planar configuration again yielding a straight dimer (motif 1) via a cyclodehydrogenation process[58] that connects the unreacted *meso* and *β* carbons. Such flipping processes, which appear plausible due to the reaction temperature being close to the porphine desorption temperature,[32] can explain the prevalence of the straight dimer (motif 1) despite steric hindrance for straight in-plane coupling.[16] Alternatively, in-plane rotation of a porphine unit of the dimer in motif 4 could entail dehydrogenation and coupling of the *β* and *meso* carbons toward formation of motif 3. Nonetheless, from the existence of motif 2 it must be inferred that also coupling mechanisms involving methine sites in an initial phase must also exist. Metal adatoms can potentially play a role in the coupling,[29,33] but our measurements gave no evidence for the occurence of any organometallic intermediates. Finally, it is interesting to note that during the course of the intermolecular coupling scenario, some macrocycles also underwent self-metalation with substrate Ag atoms,[59,60] which is revealed by the bright appearance of the molecules' centers in the STM images in Figure 2a,d (see sect. S2 in the Supporting Information for a detailed discussion).

The second key aspect of the work concerns the formation of porphine-GNR heterosystems. Following the on-surface synthesis protocol for armchair nanoribbons of width N=7 on Au(111)[26] based on 10,10′-dibromo-9,9′-bianthryl (DBBA) precursors, we realized similar GNRs on Ag(111) with significantly shorter extension (Figure 3), providing well-defined terminations.

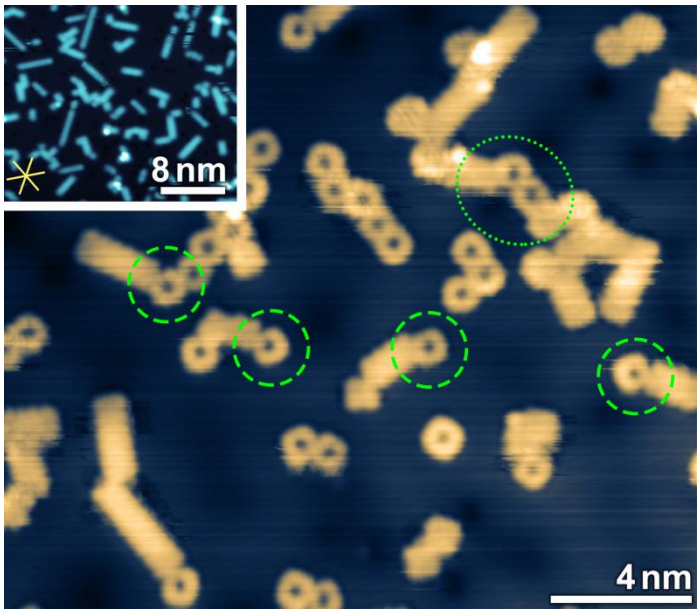

Figure 3. Fabrication of covalent porphine-GNR hybrid systems on Ag(111). STM image recorded after inducing dehydrogenative coupling reactions by porphine deposition on a surface with prefabricated GNRs (inset) held at 670 K. Coupling between porphines and GNRs is frequently observed (green dashed circles). Homocoupling of porphines and formation of complex hybrid structures, such as GNR-porphine-porphine-GNR (green dotted ellipse), is also seen. The dense-packed high-symmetry directions of the Ag(111) substrate are indicated by the yellow lines in the inset. Scan parameters: V_S = 0.09 V, I = 200 pA; inset: V_S = 1.04 V, I = 100 pA; T = 6 K.

Coupling of porphines with the prefabricated GNRs was induced by deposition of porphines onto the substrate held at 670 K, which gave rise to a large number of covalently coupled reaction products (cf. similar results for porphine homocoupling[32]). STM measurements of the resulting Ag(111) surface show that a sizeable fraction of the porphines is directly attached to the GNR (green circles in Figure 3). Coupling of porphines to GNR edges is seen predominantly at the termini of the ribbons. Similar as in the case of porphine attachment to graphene edges,[61] several distinct hetero-coupling motifs exist. In addition, the annealing again triggered self-metalation of porphines with Ag atoms[32,59,60] and dehydrogenative homocoupling[32] leading to more complex hybrid compounds, such as interconnected GNR-porphine-porphine-GNR structures (see also sect. S4 in the Supporting Information).

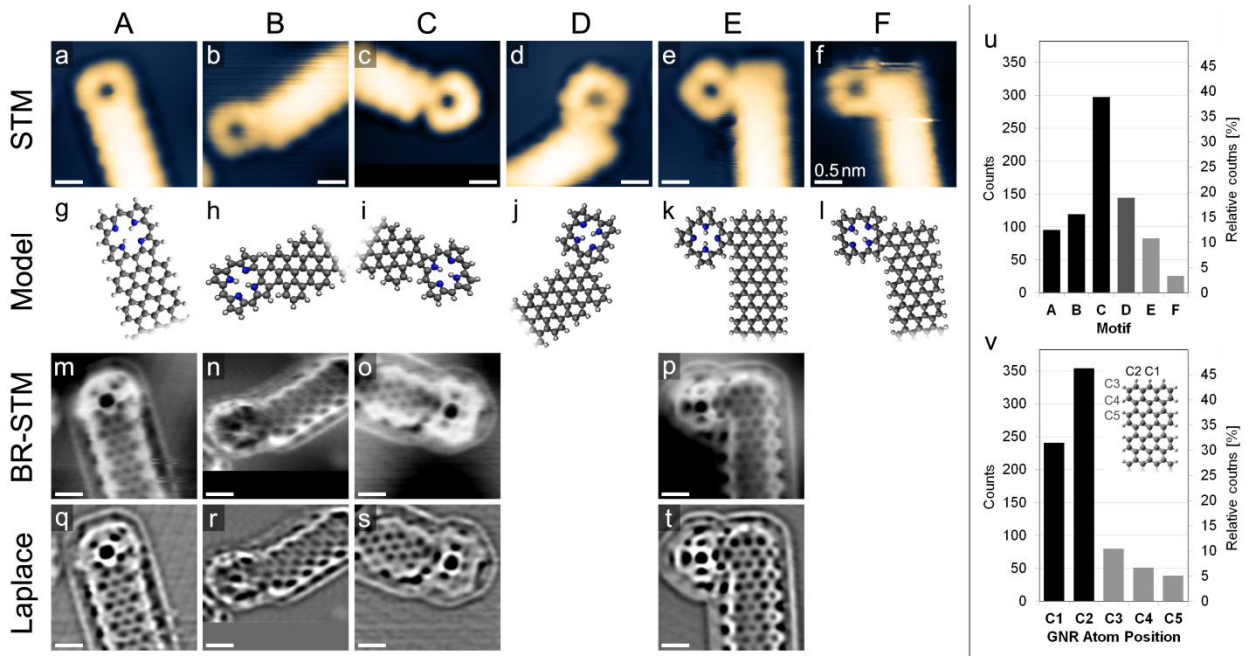

Figure 4. Main covalent coupling motifs between porphines and GNRs. **(a)-(f)** STM images of different configurations. **(g)-(l)** Proposed schematic models illustrating the coupling configurations. **(m)-(p)** Bond-resolved STM measurements employing CO-tip-functionalization and lock-in measurements (see text for description of the method). **(q)-(t)** Laplace-filtered images of (m)-(p). The bond-resolved images are in agreement with the covalent coupling motifs derived from the STM data. **(u)** Statistical analysis of the relative abundance of the porphine-GNR coupling motifs. **(v)** Statistical analysis of the GNR carbon atoms that participate in the coupling. The statistics are based on analysis of 360 coupling events. Scan parameters: (a) V_S = 40 mV, I = 100 pA; (b) V_S = 107 mV, I = 196 pA; (c),(d) V_S = 40 mV, I = 100 pA; (e) V_S = 45 mV, I = 100 pA; (f) V_S = 500 mV, I = 196 pA; (m) V_S = 40 mV, I = 100pA, V_{mod} = 26 mV r.m.s.; (n) V_S = 50 mV, I = 196 pA, V_{mod} = 28 mV r.m.s.; (o) V_S = 40 mV, I = 100 pA, V_{mod} = 26 mV r.m.s.; (p) V_S = 45 mV, I = 100 pA, V_{mod} = 26 mV r.m.s.; T = 6 K.

The main covalent coupling motifs between porphines and GNRs are shown in Figure 4. The first two rows of Figure 4 show the STM data together with the derived tentative structural models. The motifs A, B, C, and D reveal the preferred bonding of porphines to the short zigzag edge of the GNRs. In the configurations E and F porphines are coupled to the long armchair edge of the GNRs. For configuration A (Figure 4,a,g,m,q), the porphine is triply fused to the short zigzag edge of the GNR in a parallel fashion, *i.e.*, *β*-, *meso*-, *β*-carbons of the porphine are aligned with C2-, C1-, C2-carbons of the GNR. For configuration B with only two C-C bonds (Figure 4b,h,n,r), the the porphine unit is simply offset by one site. For configuration C (Figure 4c,i,o,s), two C-C bonds are formed between two adjacent porphine *β*-carbons and the C2-, C1-carbons of the GNR. In configuration D (Figure 4d,j), the porphine's *β*- and *meso*-carbons form two C-C bonds with C2-, C3-carbons of the GNR. In configurations E and F the long armchair edge of the GNR is connected, either (Figure 4e,k,p,t) with two *β*-carbons of the porphine coupled to C4- and C5-sites or (Figure 4f,l), with *β*- and *meso*-carbons of the porphine merged to C3-, C4-carbons of the GNR.

The chemical structure of selected structures of porphine-GNR junctions were confirmed using bond-resolved STM measurements (BR-STM).[7,9–13] Here the CO-functionalized tip was scanned in constant-current mode across the molecule. The applied sample bias (typical values of 40 mV) is modulated by an AC voltage (typically 25 mV r.m.s.) and the out-of-phase lock-in signal is plotted (see Supplementary Information for more details). The third row and fourth in Figure 4 shows the raw data and its contrast enhancement by Laplace-filtering, respectively. The carbon backbone of the GNRs is thereby nicely resolved, and also the pyrrole rings and the centers of the porphines show a distinct contrast. The bond structure revealed in these measurements corroborates the proposed coupling motifs. However, imaging artefacts are evident at the periphery of GNRs and porphines, presumably induced by the locally rather abrupt change of the tip height while scanning with activated z-feedback.

Statistical analysis of the observed coupling motifs underscores the preferential decoration of the short zigzag edges of the GNRs with the porphines (Figure 4u,v). In particular, the C1 and C2 carbon atoms of the GNRs partake in more than 75% of all observed coupling motifs. The C1 atom is thus identified as the most reactive GNR site. This can be explained by chemical activation of the C1 carbon atom by debromination[16] (which also can lead to passivation by hydrogen in a concurrently interfering reaction pathway[48,51,62]) or the electronic structure at this GNR edge.[63–66] Furthermore, the registry of the reactants on the surface, as well as the aspect ratio of the GNRs – causing a preference of tilting around the long axis whereby steric repulsion of reactants can be reduced when coupling occurs at the short zigzag edge – might play a role. The most common coupling motif, with a relative abundance of almost 40%, is configuration C. Herein two β-carbons of the porphine attach to the zigzag edge of the GNR, resulting in a ~45° rotated alignment of the porphine with respect to the graphene edge. Generally, nonparallel alignments are preferred (~70%) for porphine-GNR coupling. This stands in contrast with porphine-porphine coupling, where parallel alignment prevails.[32] The different reaction temperatures used in these two experiments might have an influence on the coupling: previous studies revealed that the preference for parallel porphine coupling decreased at higher reaction temperatures.[32] Furthermore, the reactivity of the C1 carbon of the GNRs can play a decisive role for the coupling. Conceivably, the most likely initial coupling step occurs between the GNR C1 site and the sterically easier accessible β-carbon of the adsorbed porphine. Further dehydrogenation and formation of C-C bonds between the GNR-C2-carbon and another porphine-β-carbon will then yield the most common coupling motif C.

In summary, we explored the bond formation in surface-assisted porphine-porphine and porphine-GNR coupling schemes at the atomic level. Distinct coupling motifs were unambiguously identified in both of these prototypical reactions, whereby an initial C-C bonding triggering a stepwise reaction can explain the preferences for the observed main reaction products. For an improved uniformity and yield of specific bond configurations refined fabrication protocols can be developed, ideally guided by insights from an in-depth theoretical analysis. Also templating effects using patterned substrates and programmed precursor self-assembly can open up novel

pathways to fabricate hybrid complex porphine/GNR systems by controllable sequential and selective coupling of optimized building blocks.

Experimental section

Experimental details are given in the Supporting Information.

Acknowledgments

This work was supported by the Munich Center for Advanced Photonics (MAP), TUM-IAS, and the ERC Advanced Grant MolArt (No. 247299) and the European Research Council Consolidator Grant NanoSurfs (No. 615233). W.A. acknowledges funding by the DFG via a Heisenberg professorship. We appreciate the introduction of the BR-STM technique by Michael F. Crommie at the On-Surface-Synthesis conference 2016. We are grateful to Profs. K. Müllen and R. Fasel for providing the GNR precursors and helpful discussions.

Keywords: C-C coupling • Dehydrogenation • Graphene nanoribbons • Porphyrins • Scanning probe microscopy • Surface chemistry

Competing interests

The authors declare no competing financial interests.

References

[1] L. Gross, F. Mohn, N. Moll, P. Liljeroth, G. Meyer, *Science* **2009**, *325*, 1110–1114.

[2] D. G. de Oteyza, P. Gorman, Y.-C. Chen, S. Wickenburg, A. Riss, D. J. Mowbray, G. Etkin, Z. Pedramrazi, H.-Z. Tsai, A. Rubio, et al., *Science* **2013**, *340*, 1434–1437.

[3] H. Mönig, S. Amirjalayer, A. Timmer, Z. Hu, L. Liu, O. Díaz Arado, M. Cnudde, C. A. Strassert, W. Ji, M. Rohlfing, et al., *Nat. Nanotechnol.* **2018**, *13*, 371–375.

[4] P. A. Held, H. Fuchs, A. Studer, *Chem. - A Eur. J.* **2017**, *23*, 5874–5892.

[5] S. P. Jarvis, *Int. J. Mol. Sci.* **2015**, *16*, 19936–59.

[6] N. Pavliček, L. Gross, *Nat. Rev. Chem.* **2017**, *1*, 0005.

[7] P. Jelinek, *J. Phys. Condens. Matter* **2017**, *29*, 343002.

[8] A. Riss, A. P. Paz, S. Wickenburg, H.-Z. Tsai, D. G. De Oteyza, A. J. Bradley, M. M. Ugeda, P. Gorman, H. S. Jung, M. F. Crommie, et al., *Nat. Chem.* **2016**, *8*, 678–683.

[9] G. D. Nguyen, H.-Z. Tsai, A. A. Omrani, T. Marangoni, M. Wu, D. J. Rizzo, G. F. Rodgers, R. R. Cloke, R. A. Durr, Y. Sakai, et al., *Nat. Nanotechnol.* **2017**, *12*, 1077–1082.

[10] P. Hapala, G. Kichin, C. Wagner, F. S. Tautz, R. Temirov, P. Jelínek, *Phys. Rev. B* **2014**, *90*, 085421.

[11] O. Krejčí, P. Hapala, M. Ondráček, P. Jelínek, *Phys. Rev. B* **2017**, *95*, 045407.

[12] E. Carbonell-Sanromà, J. Hieulle, M. Vilas-Varela, P. Brandimarte, M. Iraola, A. Barragán, J. Li, M. Abadia, M. Corso, D. Sánchez-Portal, et al., *ACS Nano* **2017**, *11*, 7355–7361.

[13] C. Weiss, C. Wagner, R. Temirov, F. S. Tautz, *J. Am. Chem. Soc.* **2010**, *132*, 11864–11865.

[14] R. Lindner, A. Kühnle, *ChemPhysChem* **2015**, *16*, 1582–1592.

[15] A. J. Weymouth, T. Hofmann, F. J. Giessibl, *Science* **2014**, *352*, 600–603.

[16] J. Cai, P. Ruffieux, R. Jaafar, M. Bieri, T. Braun, S. Blankenburg, M. Muoth, A. P. Seitsonen, M. Saleh, X. Feng, et al., *Nature* **2010**, *466*, 470–473.

[17] D. J. Rizzo, G. Veber, T. Cao, C. Bronner, T. Chen, F. Zhao, H. Rodriguez, S. G. Louie, M. F. Crommie, F. R. Fischer, *Nature* **2018**, *560*, 204–208.

[18] C. Moreno, M. Vilas-Varela, B. Kretz, A. Garcia-Lekue, M. V Costache, M. Paradinas, M. Panighel, G. Ceballos, S. O. Valenzuela, D. Peña, et al., *Science* **2018**, *360*, 199–203.

[19] A. Riss, S. Wickenburg, P. Gorman, L. Z. Tan, H.-Z. Tsai, D. G. de Oteyza, Y.-C. Chen, A. J. Bradley, M. M. Ugeda, G. Etkin, et al., *Nano Lett.* **2014**, *14*, 2251–2255.

[20] O. Gröning, S. Wang, X. Yao, C. A. Pignedoli, G. Borin Barin, C. Daniels, A. Cupo, V. Meunier, X. Feng, A. Narita, et al., *Nature* **2018**, *560*, 209–213.

[21] M. Slota, A. Keerthi, W. K. Myers, E. Tretyakov, M. Baumgarten, A. Ardavan, H. Sadeghi, C. J. Lambert, A. Narita, K. Müllen, et al., *Nature* **2018**, *557*, 691–695.

[22] J. Méndez, M. F. López, J. A. Martín-Gago, *Chem. Soc. Rev.* **2011**, *40*, 4578.

[23] F. Klappenberger, Y.-Q. Zhang, J. Björk, S. Klyatskaya, M. Ruben, J. V. Barth, *Acc. Chem. Res.* **2015**, *48*, 2140–2150.

[24] S. Kawai, S. Nakatsuka, T. Hatakeyama, R. Pawlak, T. Meier, J. Tracey, E. Meyer, A. S. Foster, *Sci. Adv.* **2018**, *4*, eaar7181.

[25] X.-Y. Wang, M. Richter, Y. He, J. Björk, A. Riss, R. Rajesh, M. Garnica, F. Hennersdorf, J. J. Weigand, A. Narita, et al., *Nat. Commun.* **2017**, *8*, 1948.

[26] S. Mishra, M. Krzeszewski, C. A. Pignedoli, P. Ruffieux, R. Fasel, D. T. Gryko, *Nat. Commun.* **2018**, *9*, 1714.

[27] T. E. Shubina, *Adv. Inorg. Chem.* **2010**, *62*, 261–299.

[28] M. Schwarz, M. Garnica, D. A. Duncan, A. Pérez Paz, J. Ducke, P. S. Deimel, P. K. Thakur, T.-L. Lee, A. Rubio, J. V. Barth, et al., *J. Phys. Chem. C* **2018**, *122*, 5452–5461.

[29] M. S. Dyer, A. Robin, S. Haq, R. Raval, M. Persson, J. Klimeš, *ACS Nano* **2011**, *5*, 1831–1838.

[30] K. Diller, F. Klappenberger, F. Allegretti, A. C. Papageorgiou, S. Fischer, A. Wiengarten, S. Joshi, K. Seufert, D. Écija, W. Auwärter, et al., *J. Chem. Phys.* **2013**, *138*, 154710.

[31] F. Hanke, S. Haq, R. Raval, M. Persson, *ACS Nano* **2011**, *5*, 9093–9103.

[32] A. Wiengarten, K. Seufert, W. Auwärter, D. Ecija, K. Diller, F. Allegretti, F. Bischoff, S. Fischer, D. A. Duncan, A. C. Papageorgiou, et al., *J. Am. Chem. Soc.* **2014**, *136*, 9346–9354.

[33] S. Haq, F. Hanke, M. S. Dyer, M. Persson, P. Iavicoli, D. B. Amabilino, R. Raval, *J. Am. Chem. Soc.* **2011**, *133*, 12031–12039.

[34] M. P. O'Neil, M. P. Niemczyk, W. A. Svec, D. Gosztola, G. L. Gaines, M. R. Wasielewski, *Science* **1992**, *257*, 63–65.

[35] V. Lin, S. DiMagno, M. Therien, J. M. Tour, *Science* **1994**, *264*, 1105–1111.

[36] N. Algethami, H. Sadeghi, S. Sangtarash, C. J. Lambert, *Nano Lett.* **2018**, *18*, 4482–4486.

[37] H. S. Cho, D. H. Jeong, S. Cho, D. Kim, Y. Matsuzaki, K. Tanaka, A. Tsuda, A. Osuka, *J. Am. Chem. Soc.* **2002**, *124*, 14642–14654.

[38] D. Y. Kim, T. K. Ahn, J. H. Kwon, D. Kim, T. Ikeue, N. Aratani, A. Osuka, M. Shigeiwa, S. Maeda, *J. Phys. Chem. A* **2005**, *109*, 2996–2999.

[39] A. A. Ryan, M. O. Senge, *European J. Org. Chem.* **2013**, *2013*, 3700–3711.

[40] A. Osuka, H. Shimidzu, *Angew. Chemie Int. Ed. English* **1997**, *36*, 135–137.

[41] F. Bischoff, K. Seufert, W. Auwärter, S. Joshi, S. Vijayaraghavan, D. Écija, K. Diller, A. C. Papageorgiou, S. Fischer, F. Allegretti, et al., *ACS Nano* **2013**, *7*, 3139–3149.

[42] F. Albrecht, F. Bischoff, W. Auwärter, J. V. Barth, J. Repp, *Nano Lett.* **2016**, *16*, 7703–7709.

[43] W. Auwärter, D. Écija, F. Klappenberger, J. V. Barth, *Nat. Chem.* **2015**, *7*, 105–120.

[44] J. Li, N. Merino-Díez, E. Carbonell-Sanromà, M. Vilas-Varela, D. G. de Oteyza, D. Peña, M. Corso, J. I. Pascual, *Sci. Adv.* **2018**, *4*, eaaq0582.

[45] W. Perkins, F. R. Fischer, *Chem. - A Eur. J.* **2017**, *23*, 17687–17691.

[46] T. Dienel, S. Kawai, H. Söde, X. Feng, K. Müllen, P. Ruffieux, R. Fasel, O. Gröning, *Nano Lett.* **2015**, *15*, 5185–5190.

[47] P. Merino, L. Rodrigo, A. L. Pinardi, J. Méndez, M. F. López, P. Pou, R. Pérez, J. A. Martín Gago, *ACS Nano* **2014**, *8*, 3590–3596.

[48] J. van der Lit, M. P. Boneschanscher, D. Vanmaekelbergh, M. Ijäs, A. Uppstu, M. Ervasti, A. Harju, P. Liljeroth, I. Swart, *Nat. Commun.* **2013**, *4*, 2023.

[49] M. Ijäs, M. Ervasti, A. Uppstu, P. Liljeroth, J. van der Lit, I. Swart, A. Harju, *Phys. Rev. B* **2013**, *88*, 075429.

[50] Y.-W. Son, M. L. Cohen, S. G. Louie, *Phys. Rev. Lett.* **2006**, *97*, 216803.

[51] L. Talirz, P. Ruffieux, R. Fasel, *Adv. Mater.* **2016**, *28*, 6222–6231.

[52] B. Schuler, W. Liu, A. Tkatchenko, N. Moll, G. Meyer, A. Mistry, D. Fox, L. Gross, *Phys. Rev. Lett.* **2013**, *111*, 106103.

[53] M. Schwarz, A. Riss, M. Garnica, J. Ducke, P. S. Deimel, D. A. Duncan, P. K. Thakur, T.-L. Lee, A. P. Seitsonen, J. V. Barth, et al., *ACS Nano* **2017**, *11*, 9151–9161.

[54] S. Haq, F. Hanke, M. S. Dyer, M. Persson, P. Iavicoli, D. B. Amabilino, R. Raval, *J. Am. Chem. Soc.* **2011**, *133*, 12031–12039.

[55] M. Röckert, M. Franke, Q. Tariq, D. Lungerich, N. Jux, M. Stark, A. Kaftan, S. Ditze, H. Marbach, M. Laurin, et al., *J. Phys. Chem. C* **2014**, *118*, 26729–26736.

[56] L. Lafferentz, V. Eberhardt, C. Dri, C. Africh, G. Comelli, F. Esch, S. Hecht, L. Grill, *Nat. Chem.* **2012**, *4*, 215–220.

[57] A. Takagi, Y. Yanagawa, A. Tsuda, N. Aratani, T. Matsumoto, A. Osuka, T. Kawai, *Chem. Commun.* **2003**, *0*, 2986–2987.

[58] M. Treier, C. A. Pignedoli, T. Laino, R. Rieger, K. Müllen, D. Passerone, R. Fasel, *Nat. Chem.* **2011**, *3*, 61–67.

[59] K. Diller, A. C. Papageorgiou, F. Klappenberger, F. Allegretti, J. V. Barth, W. Auwärter, *Chem. Soc. Rev.* **2016**, *45*, 1629–1656.

[60] H. Marbach, *Acc. Chem. Res.* **2015**, *48*, 2649–2658.

[61] Y. He, M. Garnica, F. Bischoff, J. Ducke, M.-L. Bocquet, M. Batzill, W. Auwärter, J. V. Barth, *Nat. Chem.* **2016**, *9*, 33.

[62] L. Talirz, H. Söde, J. Cai, P. Ruffieux, S. Blankenburg, R. Jafaar, R. Berger, X. Feng, K. Müllen, D. Passerone, et al., *J. Am. Chem. Soc.* **2013**, *135*, 2060–2063.

[63] K. Nakada, M. Fujita, G. Dresselhaus, M. S. Dresselhaus, *Phys. Rev. B* **1996**, *54*, 17954–17961.

[64] L. Sun, P. Wei, J. Wei, S. Sanvito, S. Hou, *J. Phys. Condens. Matter* **2011**, *23*, 425301.

[65] M. Fujita, K. Wakabayashi, K. Nakada, K. Kusakabe, *J. Phys. Soc. Japan* **1996**, *65*, 1920–1923.

[66] K. Wakabayashi, K. Sasaki, T. Nakanishi, T. Enoki, *Sci. Technol. Adv. Mater.* **2010**, *11*, 054504.

Table of Contents Text

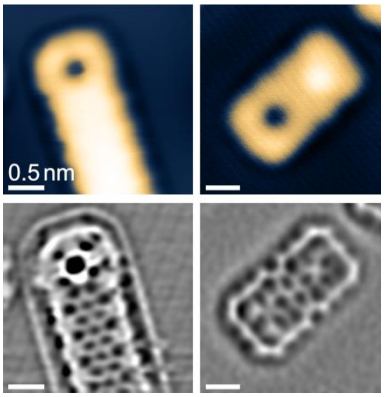

Interconnecting porphines and graphene nanoribbons: Porphine homocoupling and covalent attachment of porphines to graphene nanoribbons under atomistically well-defined on-surface conditions was investigated by bond-resolved scanning tunneling and atomic force microscopy techniques. The explored thermally induced reactions on Ag(111) afford distinct coupling motifs, the relative abundance of which is associated with stepwise reaction mechanisms.